Article

Immunity

The Energy Sensor AMPK Regulates T Cell Metabolic Adaptation and Effector Responses In Vivo

Graphical Abstract

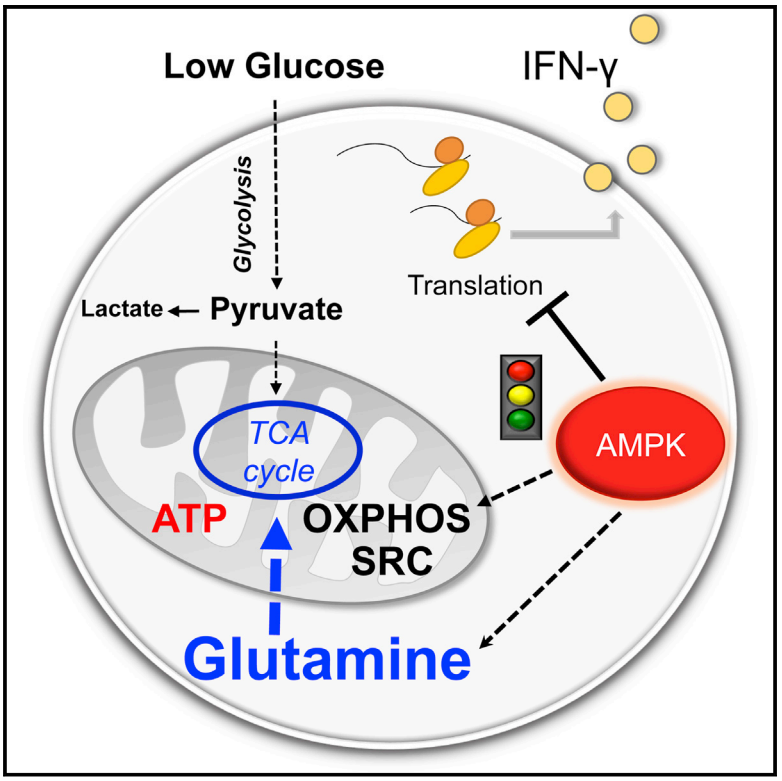

Authors

Julianna Blagih, François Coulombe, ..., Maziar Divangahi, Russell G. Jones

Correspondence

russell.jones@mcgill.ca

In Brief

T cells undergo metabolic reprogramming upon activation to fuel T cell growth, proliferation, and effector function. Jones and colleagues show effector T cells adapt their metabolic programs in response to reduced glucose availability, which is regulated by the energy sensor AMPK.

Highlights

- T cells display metabolic flexibility in response to nutrient limitation
- AMPK couples nutrient availability to T cell effector function
- T cell metabolic adaptation is AMPKα1-dependent
- AMPKα1 is required for primary T cell responses and cellular bioenergetics in vivo

Blagih et al., 2015, Immunity *42*, 41–54
January 20, 2015
http://dx.doi.org/10.1016/j.immuni.2014.12.030

CellPress

Immunity
Article

The Energy Sensor AMPK Regulates T Cell Metabolic Adaptation and Effector Responses In Vivo

Julianna Blagih,[1,2] François Coulombe,[3] Emma E. Vincent,[1] Fanny Dupuy,[1,4] Gabriela Galicia-Vázquez,[1,4] Ekaterina Yurchenko,[5,6] Thomas C. Raissi,[1,2] Gerritje J.W. van der Windt,[7] Benoit Viollet,[8,9,10] Erika L. Pearce,[7] Jerry Pelletier,[1,4] Ciriaco A. Piccirillo,[5,6] Connie M. Krawczyk,[1,5] Maziar Divangahi,[3] and Russell G. Jones[1,2,*]
[1]Goodman Cancer Research Centre, McGill University, Montreal, QC, H3G 1Y6, Canada
[2]Department of Physiology, McGill University, Montreal, QC, H3G 1Y6, Canada
[3]Departments of Medicine, Microbiology & Immunology, and Pathology, McGill International TB Centre, McGill University Health Centre and Research Institute, Meakins-Christie Laboratories, Montreal, QC, H2X 2P2, Canada
[4]Department of Biochemistry, McGill University, Montreal, QC, H3G 1Y6, Canada
[5]Department of Microbiology and Immunology, McGill University, Montreal, QC, H3A 2B4, Canada
[6]McGill University Health Centre Research Institute, Montreal General Hospital, Montreal, QC, H3G 1A4, Canada
[7]Department of Pathology & Immunology, Washington University School of Medicine, St. Louis, MO, 63110, USA
[8]Inserm, U1016, Institut Cochin, Sorbonne Paris Cité, Paris, France, 75014
[9]CNRS, UMR 8104, Sorbonne Paris Cité, Paris, France, 75014
[10]Université Paris Descartes, Sorbonne Paris Cité, Paris, France, 75014
*Correspondence: russell.jones@mcgill.ca
http://dx.doi.org/10.1016/j.immuni.2014.12.030

SUMMARY

Naive T cells undergo metabolic reprogramming to support the increased energetic and biosynthetic demands of effector T cell function. However, how nutrient availability influences T cell metabolism and function remains poorly understood. Here we report plasticity in effector T cell metabolism in response to changing nutrient availability. Activated T cells were found to possess a glucose-sensitive metabolic checkpoint controlled by the energy sensor AMP-activated protein kinase (AMPK) that regulated mRNA translation and glutamine-dependent mitochondrial metabolism to maintain T cell bioenergetics and viability. T cells lacking AMPKα1 displayed reduced mitochondrial bioenergetics and cellular ATP in response to glucose limitation in vitro or pathogenic challenge in vivo. Finally, we demonstrated that AMPKα1 is essential for T helper 1 (Th1) and Th17 cell development and primary T cell responses to viral and bacterial infections in vivo. Our data highlight AMPK-dependent regulation of metabolic homeostasis as a key regulator of T cell-mediated adaptive immunity.

INTRODUCTION

T lymphocytes are central effectors of the adaptive immune response, and their function is critical for long-lasting immunity to foreign pathogens. While T cell activation initiates specific transcriptional programs that direct T cell differentiation and effector function, the regulation of cellular metabolism is also integrated into the T cell activation program (MacIver et al., 2013; Wang and Green, 2012b). Upon activation, naive T cells shift toward a pro-growth metabolic program characterized by increased glucose and amino acid metabolism (Carr et al., 2010; Frauwirth et al., 2002; Nakaya et al., 2014; Sinclair et al., 2013; Wang et al., 2011). The predominant metabolic phenotype of activated $CD4^+$ and $CD8^+$ T effector (Teff) cells in vitro is a shift to aerobic glycolysis (Michalek et al., 2011a), also known as the "Warburg Effect." Transcription factors including Myc (Wang et al., 2011), estrogen-related receptor α (ERRα) (Michalek et al., 2011b), and the liver X receptors (LXRs) (Bensinger et al., 2008) facilitate T cell metabolic reprogramming by enhancing the expression of metabolic genes downstream of TCR signaling, which allow Teff cells to meet the bioenergetic and biosynthetic requirements of cell division and effector function.

Nutrient availability can have a profound effect on T cell activation and function. Limiting glucose or glutamine in culture medium decreases the activation of naive T cells and subsequent T cell proliferation (Ardawi and Newsholme, 1983; Brand, 1985; Carr et al., 2010; Jacobs et al., 2008; Wang et al., 2011). Consequently, reduced nutrient availability during early activation impairs interferon-γ (IFN-γ) production by $CD4^+$ and $CD8^+$ Teff cells in vitro (Cham et al., 2008; Cham and Gajewski, 2005; Chang et al., 2013). Recent work indicates that the development and function of Teff cells in vivo can be influenced by changes in nutrient transport (Macintyre et al., 2014; Nakaya et al., 2014; Sinclair et al., 2013). However, the mechanisms by which T cells couple changes in nutrient availability to immunologic function remain poorly understood. This is an important issue, as effective adaptive immunity requires Teff cells to expand, survive, and maintain effector function in a range of microenvironments, including sites of infection or inflammation where nutrients and oxygen might be limiting (McNamee et al., 2013; Sitkovsky and Lukashev, 2005). Here we examined the impact of nutrient availability on Teff cell metabolism and function. We provide evidence for plasticity in T cell metabolic reprogramming, a process regulated by the energy sensor AMP-activated protein kinase (AMPK).

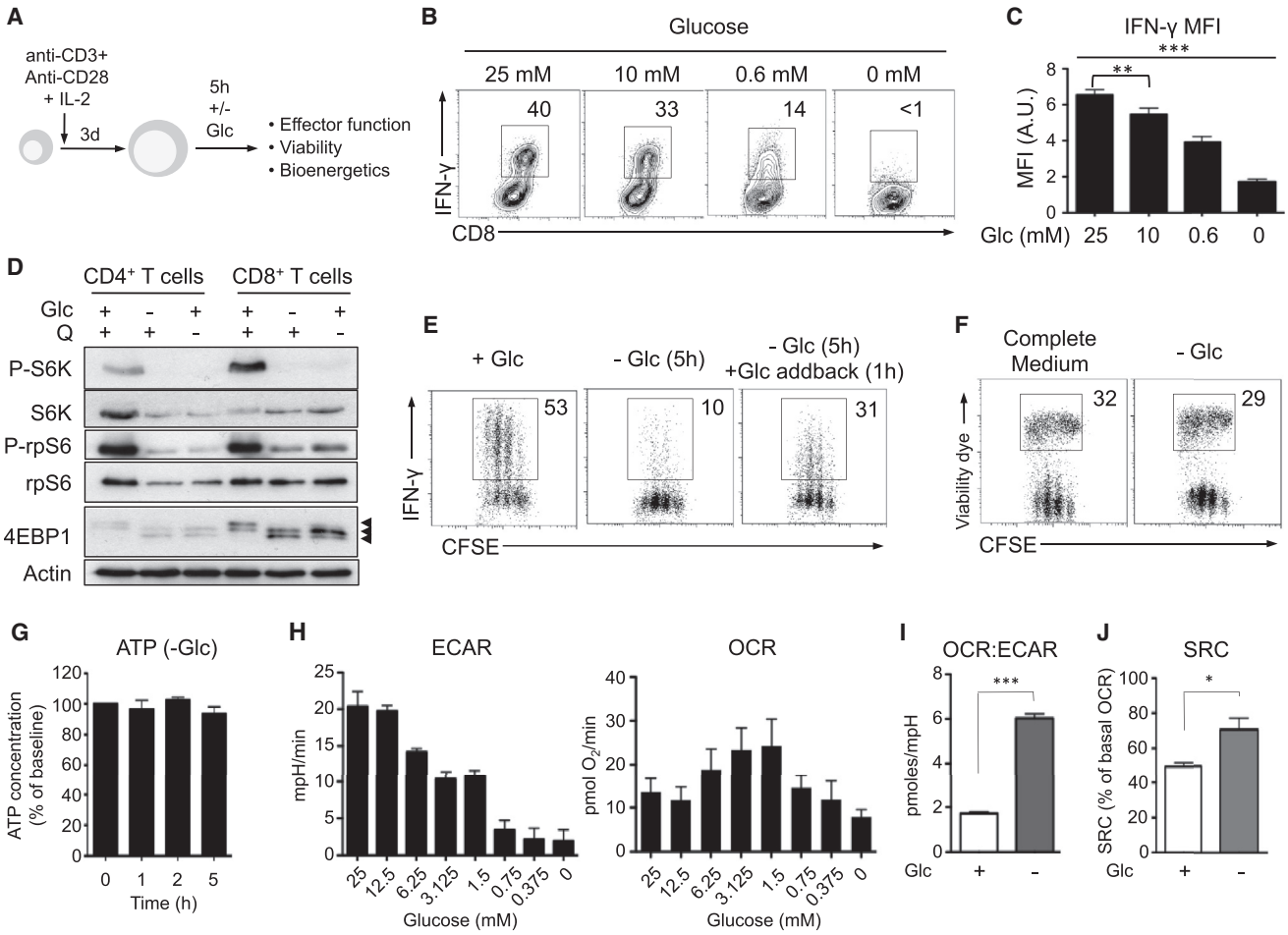

Figure 1. Glucose Limitation Induces a Metabolic Checkpoint in T Cells

(A) Schematic of T cell culture protocol.

(B) IFN-γ profiles for 3 day activated CD8$^+$ Teff cells re-stimulated under the indicated glucose concentrations.

(C) MFI of IFN-γ for cytokine producing cells in (B).

(D) Immunoblot for mTORC1 activity (total and phosphorylated S6 kinase [S6K], ribosomal protein S6 [rpS6] and total 4EBP1) in Teff cells cultured for 5 hr with or without glucose (Glc) or glutamine (Q).

(E) IFN-γ production by CFSE-labeled CD8$^+$ Teff cells cultured with (+) or without (−) glucose for 5 hr or re-fed with 25 mM glucose for 1 hr (+Glc addback, right panel). Numbers indicate the percentage of IFN-γ$^+$CD8$^+$ T cells in each culture condition.

(F) Viability of CFSE-labeled Teff cells after culture in complete or glucose-free (−Glc) medium for 5 hr (percentage of dead cells are indicated).

(G) ATP content of Teff cells after incubation in glucose-free medium for the indicated times. ATP concentration was expressed relative to ATP levels in Teff cells grown under full glucose conditions.

(H–J) Cellular bioenergetics of glucose-starved Teff cells. (H) ECAR and OCR for CD8$^+$ Teff cells cultured for 5 hr in medium containing the indicated concentrations of glucose. (I) OCR:ECAR ratio and (J) SRC for CD8$^+$ Teff cells cultured in the presence (+) or absence (−) of glucose for 5 hr. *$p < 0.05$; **$p < 0.01$; ***$p < 0.001$.

RESULTS

Glucose Limitation Induces a Metabolic Checkpoint in T Cells

In many cell types, nutrient limitation induces a metabolic checkpoint that limits cell proliferation and growth when resources are scarce. Thus, we investigated the relationship between nutrient availability, effector function, and metabolism in activated Teff cells. CD4$^+$ or CD8$^+$ Teff cells were generated via anti-CD3 and anti-CD28 antibody stimulation with interleukin-2 (IL-2) for 3 days, followed by acute glucose starvation (−Glc) for 5 hr prior to characterization (Figure 1A). Overnight glucose starvation slowed the proliferation of both CD4$^+$ and CD8$^+$ Teff cells (Figure S1A). Activated CD8$^+$ Teff cells re-stimulated under decreasing levels of glucose displayed a dose-dependent decrease in IFN-γ production (Figure 1B). Reducing glucose concentrations below 25 mM (standard concentration in IMDM) decreased both the percentage of IFN-γ$^+$ CD8$^+$ T cells (Figure 1B) and the mean fluorescence intensity (MFI) of IFN-γ staining for IFN-γ$^+$ cells (Figure 1C). This decrease in IFN-γ protein production was not due to decreased transcription of *Ifng* mRNA (Figure S1B).

A central regulator of T cell mRNA translation and effector function is the mammalian target of rapamycin complex 1 (mTORC1) (Powell and Delgoffe, 2010; Zeng and Chi, 2013). Withdrawal of either glucose or glutamine suppressed mTORC1 activity in activated T cells, as measured by reduced phosphorylation of the mTORC1 targets S6K, rpS6, and 4E-BP1 (Figure 1D). Total S6K protein was also reduced in T cells starved of glucose or glutamine (Figure 1D).

We next assessed whether the effect of glucose availability on T cell cytokine production was reversible. $CD8^+$ Teff cells were starved of glucose for 5 hr, followed by re-introduction of 25 mM glucose for 1 hr, and IFN-γ production by Teff cells was measured by flow cytometry. While glucose withdrawal promoted a 5-fold reduction in the frequency of IFN-γ^+ $CD8^+$ T cells, re-introduction of glucose for 1 hr restored the ability of glucose-starved Teff cells to produce IFN-γ (Figure 1E). Teff cell viability was maintained during this culture period despite acute removal of glucose (Figure 1F).

Finally, we examined the effect of glucose availability on T cell metabolism. Cellular ATP concentrations were maintained in T cells after acute glucose starvation (Figure 1G). To explore this further, we cultured Teff cells for 5 hr under various glucose concentrations, and assessed their bioenergetic profiles via Seahorse assay (Wu et al., 2007). The extracellular acidification rate (ECAR), a measure of extracellular pH that positively co-relates with glycolysis in lymphocytes (Chang et al., 2013), decreased in $CD8^+$ T cells as glucose concentration decreased, despite the presence of IL-2 to drive glycolysis (Figure 1H). In parallel, we examined the mitochondrial O_2 consumption rate (OCR), a measure of OXPHOS. We found that mitochondrial OCR was maximal in $CD8^+$ T cells at lower glucose concentrations (1.5–6 mM), and largely maintained under glucose-free conditions (Figure 1H). This translated as a progressive increase in the OCR:ECAR ratio as glucose concentrations decreased (Figure S1C). Both $CD8^+$ and $CD4^+$ T cells demonstrated a sharp decline in ECAR while increasing their OCR:ECAR ratio under glucose-free conditions (Figures 1H and 1I and S1D and S1E), consistent with previous results (Chang et al., 2013; Sukumar et al., 2013).

Mitochondrial spare respiratory capacity (SRC) is defined as the increase in OCR following uncoupling with FCCP (van der Windt et al., 2012). SRC is the maximum oxidative potential of the mitochondria available for energy production, and is linked with increased bioenergetic advantage in T cells during recall responses and metabolic stress (van der Windt et al., 2012; van der Windt et al., 2013). Glucose starvation promoted an increase in SRC in Teff cells (Figures 1J and S1E). Together these data indicate that T cells display flexibility in their metabolic reprogramming in response to changing glucose availability.

Glutamine Supports T Cell Metabolism under Conditions of Glucose Limitation

Given that ATP concentrations are maintained in glucose-starved Teff cells despite reduced glycolysis, we hypothesized that Teff cells engage alternate metabolic pathways to maintain cellular bioenergetics. The non-essential amino acid glutamine is critical for activation-induced T cell proliferation (Carr et al., 2010; Wang et al., 2011) and is used in many cell types to fuel oxidative metabolism under stress conditions (Le et al., 2012; Yang et al., 2009). Glutamine withdrawal reduced the OCR of Teff cells despite the continued presence of glucose (Figure S2A), resulting in a decreased OCR:ECAR ratio (Figure 2A). Glutamine withdrawal had only a minor effect on the ECAR of Teff cells (Figure S2A). However, unlike glucose, glutamine was required to maintain ATP concentrations in Teff cells (Figure 2B). The expression of genes involved in glutamine metabolism, including the glutamine transporters *Snat1* and *Snat2* and glutaminase (*Gls*), increased significantly in Teff cells under glucose withdrawal (Figure 2C), while glycolytic gene expression was largely unaffected (Figure S2B).

We next conducted stable isotope tracer analysis (SITA) with [U-^{13}C]-glutamine to assess whether glutamine metabolism in T cells was altered by glucose availability (schematic in Figure S2C). Teff cells were acutely starved of glucose, followed by culture for an additional hour with [U-^{13}C]-glutamine (in glucose-free medium), and ^{13}C incorporation in metabolite pools was quantified by GC-MS. This approach allowed us to measure the incorporation of ^{13}C label into lactate and TCA cycle metabolites as they are approaching steady-state labeling (Figure S2D). Total concentrations of [U-^{13}C]-glutamine-derived glutamate were elevated in glucose-starved Teff cells (Figure 2D), while similar concentrations of ^{13}C enrichment were observed in succinate, fumarate, and malate between control and glucose-starved Teff cells (Figure 2E), indicating that glutamine-derived TCA cycle metabolites were maintained in glucose-starved Teff cells. In contrast, Teff cells starved of glutamine displayed a depletion of TCA cycle intermediates that could not be compensated by glucose (Figure S2E). Citrate concentrations decreased under glucose deprivation (Figure 2E), which might reflect the reduced contribution of glucose to the citrate pool. The distribution of mass isotopomers in [U-^{13}C]-glutamine-derived TCA cycle metabolites was not dramatically affected by glucose availability (Figure S2F).

Glucose-derived pyruvate is an important source of acetyl-CoA, which is a key carbon input into the TCA cycle (Owen et al., 2002). Conventional formation of malate from [U-^{13}C]-glutamine in the TCA cycle will generate malate m+4. However, decarboxylation of glutamine-derived malate (or OAA) will generate pyruvate m+3 due to the loss of one carbon as CO_2 (Figure S2C). If the latter pathway is active, condensation of [U-^{13}C]-glutamine-derived acetyl-CoA m+2 (from PDH-mediated decarboxylation of pyruvate m+3) with [U-^{13}C]-glutamine-derived OAA (m+4) is predicted to generate citrate m+6 (Figure S2C). Interestingly, we found that the proportion of pyruvate m+3 increased specifically in glucose-starved Teff cells (Figures 2F and S2F). Similarly, citrate m+6 was generated only in Teff cells deprived of glucose (Figures 2G and S2F). Finally, activated Teff cells that are normally resistant to acute glucose withdrawal (Figure 1F) displayed increased levels of cell death when both glucose and glutamine were absent from the culture medium (Figure 2H). Collectively, these data highlight a central role for glutamine in maintaining T cell metabolism and viability.

AMPK Regulates T Cell Effector Function in Response to Nutrient Availability

AMPK is a central regulator of cellular responses to metabolic stress (Hardie et al., 2012) and is activated in $CD8^+$ T cells during primary responses in vivo (Pearce et al., 2009). Similar to

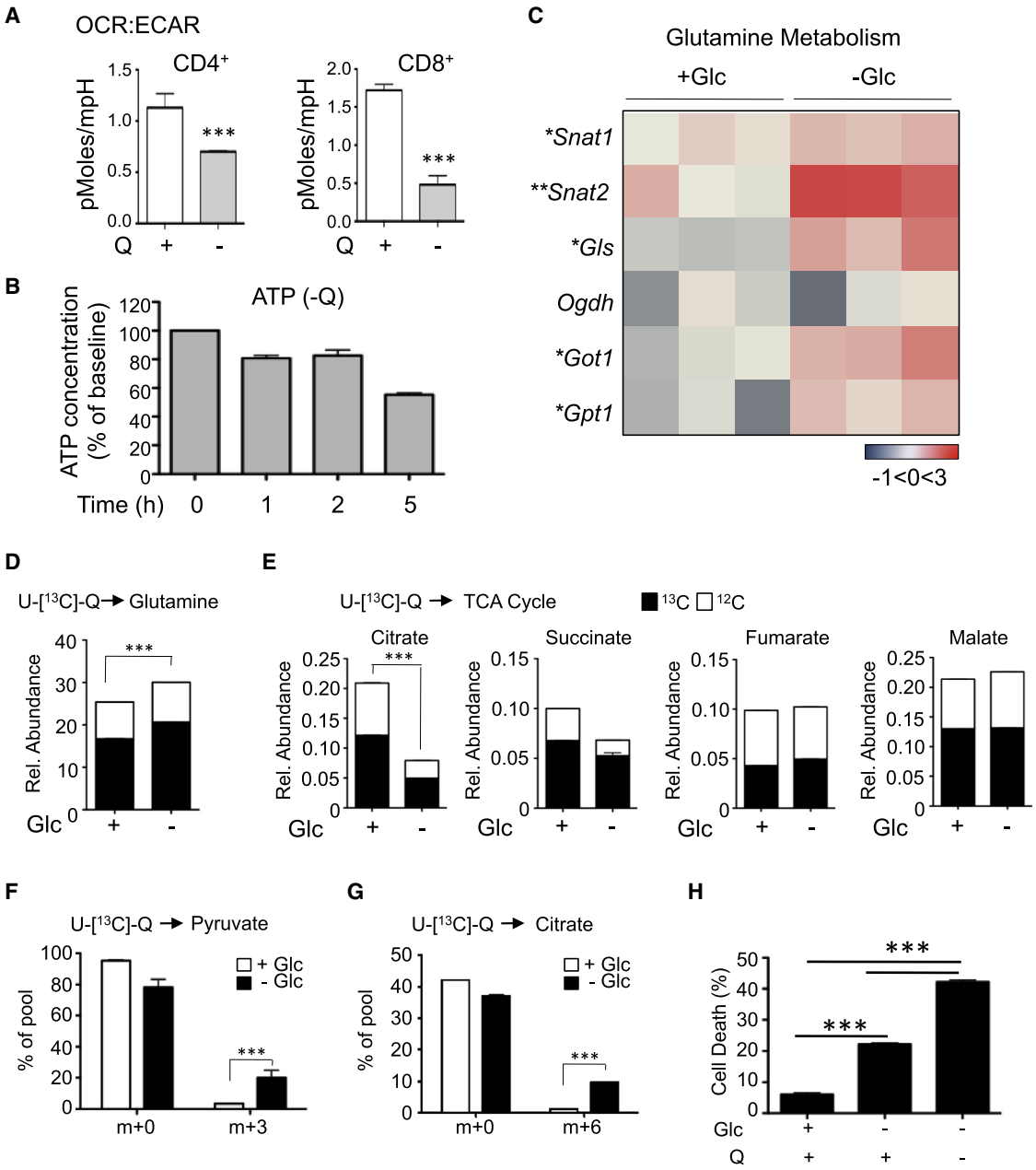

Figure 2. Glutamine Supports T Cell Metabolism under Conditions of Glucose Limitation

(A) OCR:ECAR ratio for Teff cells cultured for 5 hr under control (+Q, white) or glutamine-free (−Q, gray) conditions.

(B) ATP concentrations in Teff cells after culture in glutamine-free medium (−Q) for the indicated times. Data are expressed relative to ATP concentrations in Teff cells grown with 4 mM glutamine.

(C) Expression of glutamine metabolism genes by $CD8^+$ Teff cells cultured with (+) or without (−) glucose for 5 hr. Data are expressed as the log2 of fold changes from $CD8^+$ Teff cells grown in complete medium (n = 3 mice per condition).

(D) Relative abundance of ^{13}C-labeled (black) or unlabeled (white) glutamate in Teff cells following culture with (+) or without (−) glucose (Glc) for 5 hr, followed by 1 hr incubation with medium containing 2mM [U-^{13}C]-Q. Metabolite abundances were determined by GC-MS, and expressed as the mean ± SEM for triplicate samples.

(E) Relative abundance of ^{13}C-labeled (black) or unlabeled (white) TCA cycle intermediates citrate, succinate, fumarate, and malate for Teff cells treated as in (D).

(F and G) Mass isotopomer distribution of [U-^{13}C]-glutamine-derived carbon into pyruvate and citrate. Teff cells were cultured as in (D) and the percent distribution of m+3 pyruvate (F) and m+6 citrate (G) determined by GC-MS. The data represent the percent abundance of the indicated isotopomers for their respective metabolite pool.

(H) $CD8^+$ Teff cell viability following culture with (+) or without (−) glucose (Glc) or glutamine (Q) for 12 hr. *p < 0.05; **p < 0.01; ***p < 0.001.

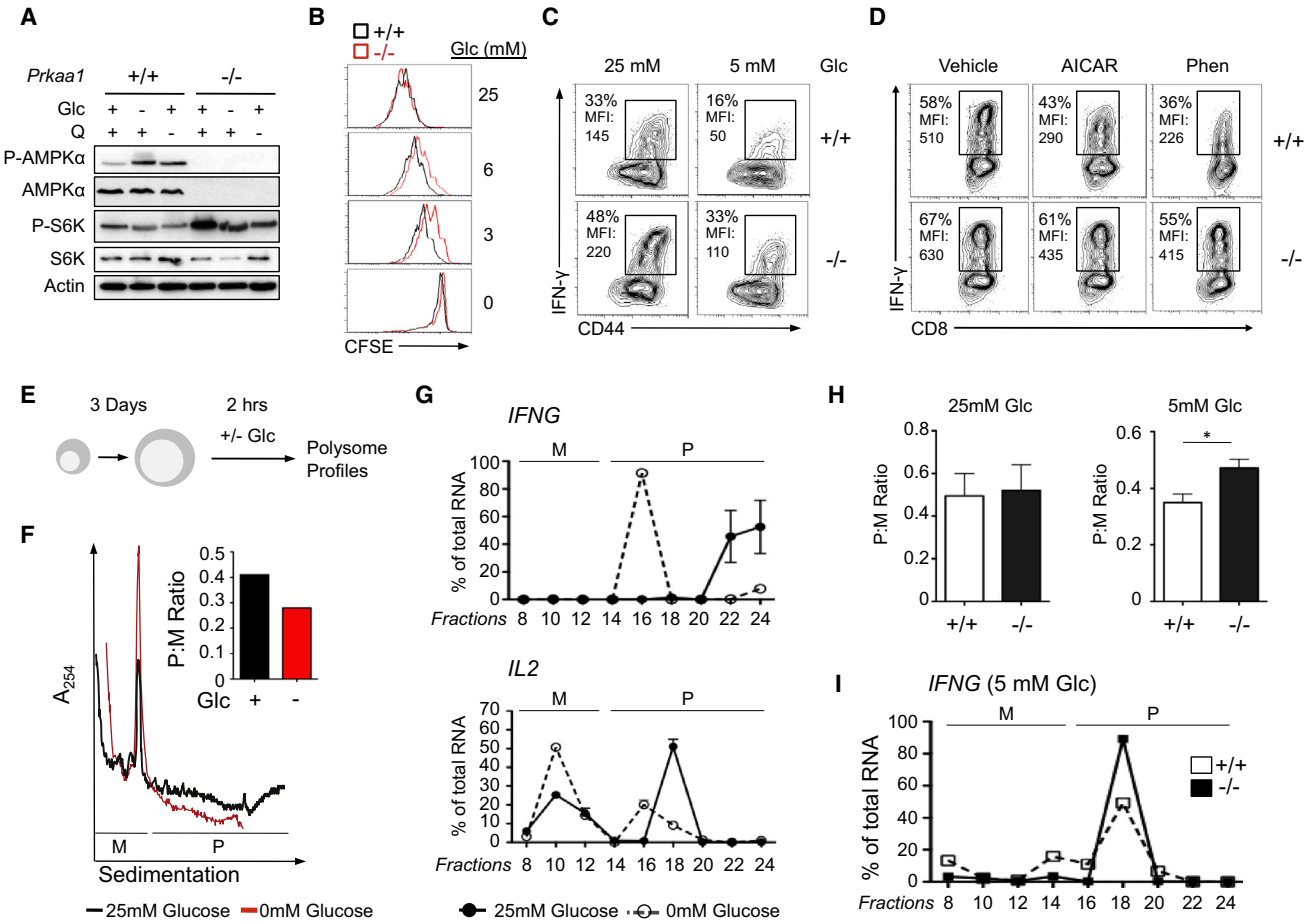

Figure 3. AMPK Regulates T Cell Effector Function in Response to Nutrient Availability

(A) Immunoblot for AMPK activation (total and phospho-AMPKα) and mTORC1 activation (total and phospho-S6K) in wild-type (+/+) or *Prkaa1*-deficient (−/−) T cells cultured with or without glucose (Glc) or glutamine (Q) for 5 hr.

(B) Proliferation of CFSE-labeled *Prkaa1*$^{+/+}$ and *Prkaa1*$^{-/-}$ CD4^{+} T cells 3 days after stimulation with αCD3 and αCD28 antibodies plus irradiated splenocytes in medium containing the indicated glucose concentrations.

(C) IFN-γ production by *Prkaa1*$^{+/+}$ or *Prkaa1*$^{-/-}$ CD8^{+} Teff cells re-stimulated with PMA and ionomycin in medium containing 25 or 5 mM glucose. The percentage of IFN-γ^{+} cells (of total CD8^{+} cells) and the MFI of IFN-γ staining are indicated.

(D) IFN-γ production by control *Prkaa1*$^{+/+}$ or *Prkaa1*$^{-/-}$ CD8^{+} Teff cells following treatment with AICAR (2 mM) or Phenformin (Phen, 2 mM).

(E) Schematic of experimental setup for polysomal fractionation.

(F) Teff cells were treated as in (E) and cell lysates sedimented on 10% to 50% sucrose gradients. Displayed is the relative absorbance (A) at 254 nm for RNA fractions collected from Teff cells cultured in 25 mM (black) or 0 mM (red) glucose. Monosome (M) and polysome (P) fractions are indicated. Inset, the polysome-to-monosome ratio (P:M) for Teff cells cultured in 25mM (black) versus 0 mM (red) glucose.

(G) Quantitative RT-PCR (qPCR) for *Ifng* and *Il2* mRNAs associated with monosome (M) and polysome (P) fractions. Total mRNA was purified from each fraction in (F) and qPCR for mRNAs was performed on the indicated fractions. Data are presented as the percentage of mRNA in each fraction of the total RNA pool.

(H) P:M ratio for *Prkaa1*$^{+/+}$ (white) or *Prkaa1*$^{-/-}$ (black) T cells restimulated under 25 or 5 mM glucose conditions.

(I) *Prkaa1*$^{+/+}$ (white) or *Prkaa1*$^{-/-}$ (black) Teff cells were cultured in 5 mM glucose and total RNA isolated from fractions were analyzed for *Ifng* expression by qPCR. Data are presented as in (G) for biological triplicate samples.

previous results (Rolf et al., 2013), Thr-172 phosphorylation of the AMPKα subunit in T cells was increased by either glucose or glutamine deprivation (Figure 3A). S6K phosphorylation was elevated in AMPKα1-deficient (*Prkaa1*$^{-/-}$) Teff cells relative to control Teff cells and remained elevated when cells were cultured in medium lacking glucose or glutamine (Figure 3A). Although control and AMPKα1-deficient T cells displayed similar proliferation rates under full glucose (25 mM) conditions, *Prkaa1*$^{-/-}$ T cells displayed reduced proliferation when stimulated under low glucose concentrations (3–6 mM) (Figure 3B). T cell viability between genotypes was not affected during these short culture periods (Figure S3A).

We next assessed the effect of glucose availability on cytokine production by *Prkaa1*$^{-/-}$ T cells. We observed an increased percentage of IFN-γ-producing CD8^{+} T cells in *Prkaa1*$^{-/-}$ T cell cultures, as well as an increase in the MFI of IFN-γ for *Prkaa1*$^{-/-}$ cytokine-producing T cells (Figure 3C). Reducing extracellular glucose to physiological concentrations (5 mM) decreased both the percentage of IFN-γ^{+} CD8^{+} T cells and the MFI of cytokine-producing T cells in control cultures, while *Prkaa1*$^{-/-}$ CD8^{+}

T cells displayed greater resistance to suppression of IFN-γ production by glucose limitation (Figure 3C). AMPK activation was sufficient to suppress IFN-γ production by Teff cells, as acute treatment with the AMPK agonists AICAR or phenformin (Phen) suppressed IFN-γ production by wild-type but not *Prkaa1*$^{-/-}$ CD8^{+} Teff cells (Figures 3D and S3B and S3C). Notably, AICAR and phenformin treatment acutely suppressed the percentage of IFN-γ^{hi} CD8^{+} T cells in culture (Figures S3B and S3C).

Given that *Ifng* mRNA levels in Teff cells were not significantly affected by glucose availability (Figure S1B), one possibility for the reduced staining intensity of IFN-γ in glucose-starved T cells was the differential translation of *Ifng* mRNA, which we assessed by polysome fractionation (Figure 3E). Polysome profiles of Teff cells cultured under glucose-free versus full glucose conditions revealed a reduction in the polysome fraction and decrease in the polysome-to-monosome (P:M) ratio in glucose-starved Teff cells (Figure 3F), indicative of reduced mRNA translation (Jaramillo et al., 2011). The majority of *Ifng* mRNA in Teff cells cultured under high-glucose conditions was associated with heavy polysome fractions (fractions 14 and above), indicating active translation of this transcript (Figure 3G, top panel). Glucose withdrawal promoted a shift in *Ifng* mRNA from heavy to light polysome fractions in Teff cells (Figure 3G), consistent with reduced translation of *Ifng* mRNAs. Similar reductions in the percentage of *Il2* (Figure 3G, bottom panel) and *Gapdh* (Figure S3D) mRNAs associated with heavy polysome fractions were observed in glucose-starved Teff cells.

We next examined the polysome profiles of *Prkaa1*$^{+/+}$ and *Prkaa1*$^{-/-}$ Teff cells grown under high (25 mM) or low (5 mM) glucose concentrations. *Prkaa1*$^{-/-}$ Teff cells maintained a higher P:M ratio than control Teff cells under low glucose conditions (Figure 3H), and a greater percentage of *Ifng* mRNA remained associated with heavy polysome fractions in AMPKα1-deficient T cells under glucose starvation conditions (Figure 3I). mRNA transcripts for *Gapdh* were similarly enriched in polysomes from glucose-starved *Prkaa1*$^{-/-}$ Teff cells (Figure S3E).

AMPK Regulates Metabolic Adaptation in Activated T Cells

We next examined the influence of AMPK on Teff cell metabolism. Under standard growth conditions, *Prkaa1*$^{-/-}$ Teff cells displayed a modest increase in OCR relative to control T cells, but no difference in ECAR (Figure S4A). Glucose starvation induced a large drop in ECAR for both control and *Prkaa1*$^{-/-}$ T cells (Figure S4B). However, both the OCR (Figure 4A) and SRC (Figure 4B) of *Prkaa1*$^{-/-}$ T cells were significantly reduced by glucose withdrawal compared to control Teff cells. Analysis of adenylate concentrations by LC-MS revealed a decreased ATP:AMP ratio in AMPKα1-deficient T cells, which decreased further under glucose withdrawal (Figure 4C). Notably, ATP concentrations were largely maintained in control T cells upon glucose withdrawal, but decreased by ~50% in *Prkaa1*$^{-/-}$ Teff cells, whereas AMP concentrations were elevated in *Prkaa1*$^{-/-}$ T cells regardless of glucose concentration (Figure S4C).

Given the dependence of OXPHOS, mitochondrial respiratory capacity, and ATP maintenance on AMPKα1 expression in Teff cells, we next assessed the impact of AMPKα1 loss on Teff cell metabolic reprogramming. *Prkaa1*$^{-/-}$ Teff cells failed to upregulate the expression of genes involved in glutamine metabolism upon glucose withdrawal and maintained expression of glucose metabolism genes including *Glut1* and *Ldha* (Figure 4D). The conversion of glutamine to glutamate, which is enhanced in Teff cells by glucose withdrawal (Figure 2D), was lower in glucose-starved *Prkaa1*$^{-/-}$ Teff cells (Figures 4E and S4D). Moreover, the total amount of glutamine-derived TCA cycle intermediates (including citrate, succinate, fumarate, and malate) was lower in *Prkaa1*$^{-/-}$ Teff cells upon glucose starvation (Figures 4F and S4D). The distribution of mass isotopomers in [U-^{13}C]-glutamine-derived metabolites was similar between control and *Prkaa1*$^{-/-}$ Teff cells (Figure S4E). However, *Prkaa1*$^{-/-}$ Teff cells displayed lower abundance of [U-^{13}C]-glutamine-derived pyruvate m+3 (Figure 4G) and citrate m+6 (Figure 4H) under conditions of glucose limitation. Finally, *Prkaa1*$^{-/-}$ CD4^{+} and CD8^{+} Teff cells displayed increased cell death in response to glucose withdrawal (Figure 4I). Together, these data indicate that AMPKα1 is required to support pathways of glutamine metabolism engaged by T cells to maintain cellular bioenergetics and T cell survival.

AMPK Is Required for the Accumulation of Th1 and Th17 Cells and Development of Colitis In Vivo

We next assessed the function of *Prkaa1*$^{-/-}$ T cells in vivo through a series of adoptive transfer experiments. Loss of AMPKα1 did not affect the ability of naive T cells to expand in vivo, as both CD4^{+} and CD8^{+} T cells from *Prkaa1*$^{-/-}$ mice underwent homeostatic proliferation in *Rag2*$^{-/-}$ hosts (Figure 5A). We next adoptively transferred naive CD4^{+}CD25^{-} T cells sorted from *Prkaa1*$^{+/+}$ or *Prkaa1*$^{-/-}$ mice into T cell-deficient (*Tcrb*$^{-/-}$) or *Rag2*$^{-/-}$ mice, and the presence of inflammatory donor CD4^{+} T cells in the colonic lamina propria (cLP) and mesenteric lymph nodes (mLNs) was measured 3 weeks later (Figure S5A). Loss of AMPKα1 did not impair the differentiation of donor-derived CD4^{+} T cells into Th1 (IFN-γ^{+}) or Th17 (IL-17^{+}) lineage cells in *Tcrb*$^{-/-}$ mice, as the frequency of Th1 or Th17 cells in the cLP and mLN was similar between animals that received control or *Prkaa1*$^{-/-}$ CD4^{+} T cells (Figures 5B and S5B). Consistent with our in vitro data linking AMPKα1 to suppression of cytokine mRNA translation (Figure 3C), the MFI of IFN-γ staining for IFN-γ^{+}CD4^{+} T cells infiltrating the cLP was significantly higher in *Prkaa1*$^{-/-}$ donor CD4^{+} T cells (Figures 5C and 5D). However, the total number of CD4^{+} T lymphocytes recovered from the mLN and cLP of recipient mice was lower in animals that received *Prkaa1*$^{-/-}$ CD4^{+} T cells (Figure S5C). This translated into a 5-fold reduction in the total number of inflammatory Th1 or Th17 cells in the mLN and cLP of mice that received naive *Prkaa1*$^{-/-}$ CD4^{+} T cells (Figure 5E). Histologic analysis of colon specimens revealed moderate-to-severe colitis in mice receiving wild-type donor CD4^{+} T cells, marked by globet cell loss and severe mononuclear infiltration into the mucosa and extension into the muscularis and serosa (Figure 5F). In contrast, the colons of mice that received *Prkaa1*$^{-/-}$ CD4^{+} T cells showed almost no colitis with intact epithelial structures and reduced inflammatory infiltrate (Figures 5F and 5G).

AMPK Is Required for Effective Primary T Cell Responses to Viral and Bacterial Infections

We next investigated the role of AMPK in T cell-mediated immune responses to viral and bacterial infections in vivo using

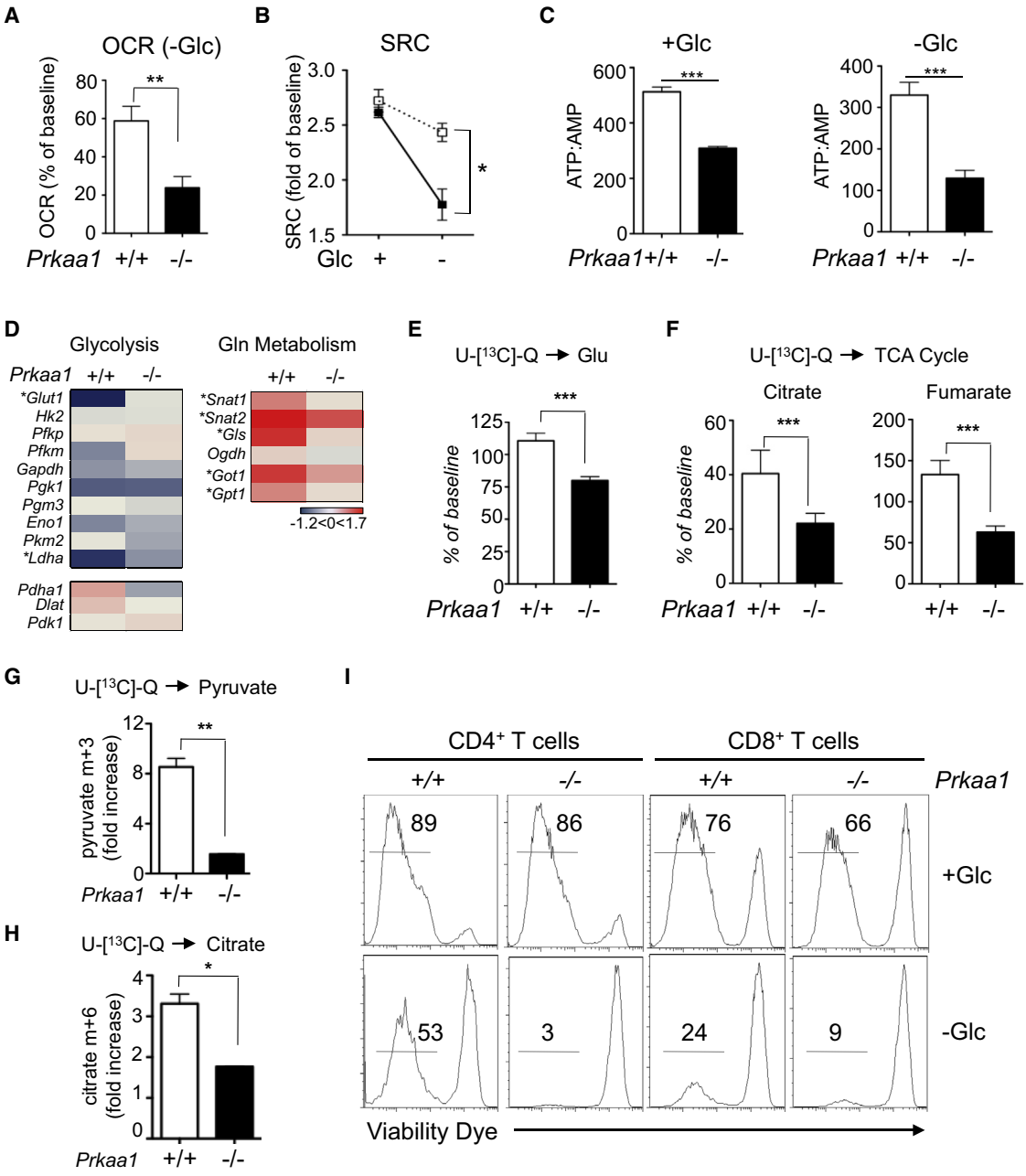

Figure 4. AMPK Regulates Metabolic Adaptation in Activated T Cells

(A and B) *Prkaa1*$^{+/+}$ (white) or *Prkaa1*$^{-/-}$ (black) Teff cells were subject to glucose withdrawal for 5 hr, and the OCR (A) and SRC (B) determined by Seahorse assay. OCR in (A) was expressed relative to the OCR of Teff cells grown in glucose-replete conditions.

(C) ATP:AMP ratio of *Prkaa1*$^{+/+}$ or *Prkaa1*$^{-/-}$ Teff cells grown under 25 mM (+) or glucose-free (–) conditions.

(D) Expression of glucose and glutamine metabolism genes in *Prkaa1*$^{+/+}$ or *Prkaa1*$^{-/-}$ T cells grown under glucose withdrawal. Data are expressed as the log2 fold change in gene expression under glucose withdrawal relative to cells grown under full-glucose conditions.

(E–H) *Prkaa1*$^{+/+}$ (white) or *Prkaa1*$^{-/-}$ (black) Teff cells were subjected to glucose withdrawal for 5 hr, and the abundance of [U-^{13}C]-glutamine (Q)-derived glutamate (E) and TCA cycle intermediates citrate and fumarate (F) were determined by GC-MS (expressed relative to +Glc conditions). The fold increase in glutamine-derived m+3 pyruvate (G) and m+6 citrate (H) was determined in T cells grown under glucose-free relative to glucose-replete conditions. (I) Viability of *Prkaa1*$^{+/+}$ or *Prkaa1*$^{-/-}$ Teff cells cultured in the presence (+) or absence (–) of glucose for 18 hr (% viable cells are indicated). *p < 0.05; **p < 0.01; ***p < 0.001.

mice with T cell-specific deletion of AMPKα1 (CD4-Cre^{+}; *Prkaa1*$^{fl/fl}$, hereafter referred to as KO-T). We first assessed pulmonary T cell-mediated immune responses by infecting KO-T mice and control littermates (WT-T) with a sub-lethal dose (~50 PFU) of influenza A virus (IAV) (Figure S6A) (Coulombe et al., 2014; Jaworska et al., 2014). At day 9 post-infection

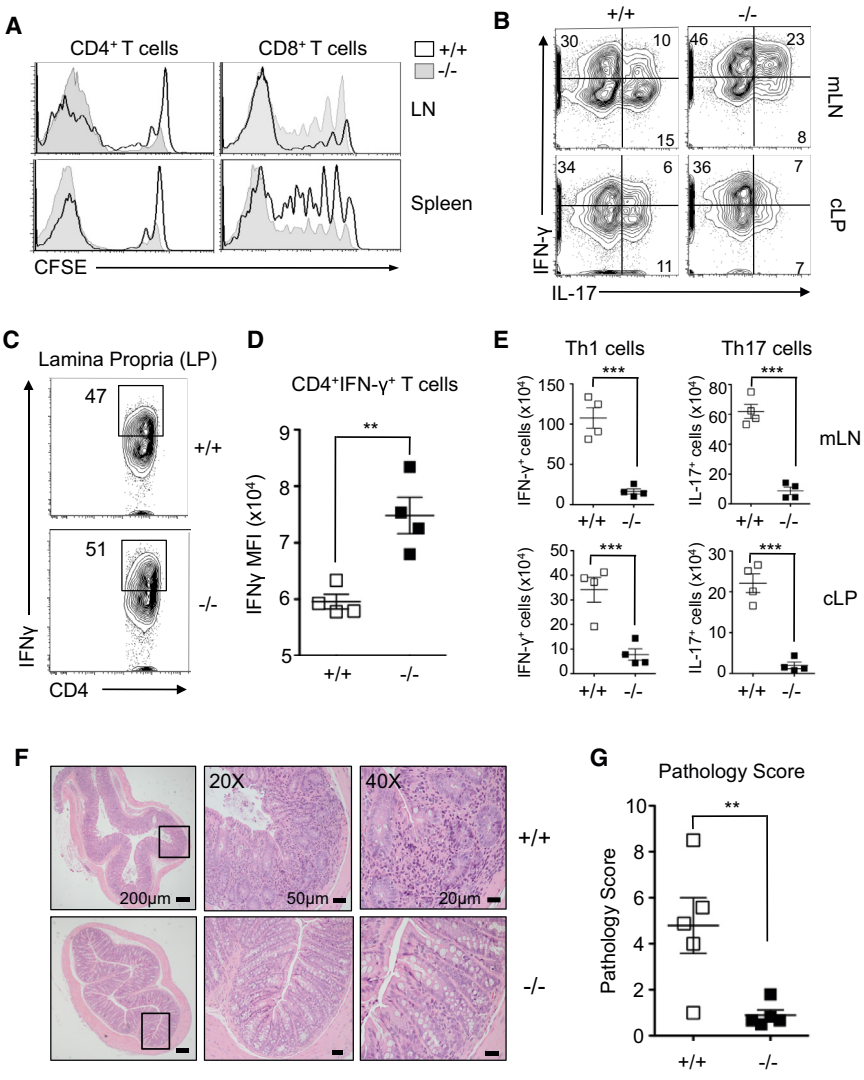

Figure 5. AMPK Is Required for the Accumulation of CD4$^+$ Th1 and Th17 Cells In Vivo

(A) CFSE dilution profiles of *Prkaa1*$^{+/+}$ (black line) and *Prkaa1*$^{-/-}$ (gray histogram) T cells 5 days following adoptive transfer into *Rag2*$^{-/-}$ mice.

(B) IFN-γ and IL-17A staining for donor CD4$^+$ cells isolated from the mLNs or cLP of recipient mice 3 weeks post transfer.

(C) IFN-γ production by donor *Prkaa1*$^{+/+}$ (white) or *Prkaa1*$^{-/-}$ (black) CD4$^+$ cells in the cLP. Numbers indicate the percentage of IFN-γ$^+$CD4$^+$ donor cells isolated from the cLP.

(D) MFI of IFN-γ staining for IFN-γ$^+$ donor CD4$^+$ T cells in (C).

(E) Total number of *Prkaa1*$^{+/+}$ (white) or *Prkaa1*$^{-/-}$ (black) Th1 (CD4$^+$IFNγ$^+$) and Th17 (CD4$^+$IL-17$^+$) cells isolated from the mLN and cLP of *Tcrb*$^{-/-}$ mice 3 weeks post-transfer.

(F) Representative H&E staining of colon sections from *Tcrb*$^{-/-}$ mice receiving naive *Prkaa1*$^{+/+}$ or *Prkaa1*$^{-/-}$ CD4$^+$ T cells 3 weeks post adoptive T cell transfer.

(G) Pathology scoring of colon sections from recipient mice. *p < 0.05; **p < 0.01; ***p < 0.001.

(dpi), the total number of leukocytes was reduced in the bronchoalveolar lavage (BAL), lungs and mediastinal lymph node (LN) of IAV-infected KO-T mice compared to littermate controls (Figure S6B). The frequency and total number of T cells was lower in the BAL and lungs of KO-T mice (Figure S6C), which was associated with decreased frequency and total numbers of CD4$^+$ and CD8$^+$ T cells (Figures 6A and S6D). In addition, the frequency and total number of CD8$^+$ T cells specific for the immunodominant IAV nucleoprotein (NP) epitope was reduced in the BAL (Figure 6B) and lungs (Figure S6E) of IAV-infected KO-T mice. In IAV-infected WT-T and KO-T mice, the frequency of pulmonary T cells producing IFN-γ was similar following stimulation with whole UV-inactivated IAV, hemagglutinin (HA) peptide (specific for CD4$^+$ T cells), or NP peptide (specific for CD8$^+$ T cells) at day 9 or 12 post-infection (Figures 6C and 6D, left panels). However, consistent with the reduced T cell numbers in infected KO-T mice, there was a reduction in the total number of IFN-γ-producing CD4$^+$ and CD8$^+$ T cells in the BAL of IAV-infected KO-T mice relative to control animals (Figures 6C and 6D, right panels). Considering the quantity and quality of innate immunity (including macrophages) is intact in KO-T mice, we observed no difference in pulmonary viral load during early phases of infection (Figure 6E).

We next investigated the role of AMPK in T cell-mediated immune responses to the Gram-positive bacterium *L. monocytogenes* (*Lm*) by infecting control and KO-T mice with a variant of *Lm* expressing OVA (*rLmOVA*) (Krawczyk et al., 2007) (Figure S7A). KO-T mice displayed a reduced number of OVA-specific CD8$^+$ T cells 7 days post infection with *rLmOVA* compared to control littermates (Figures 7A and 7B). Similar to infection with IAV, KO-T mice displayed a reduction in total CD4$^+$ and CD8$^+$ T cell numbers following *rLmOVA* infection relative to controls (Figure S7B). The reduction in OVA-specific T cells was not due to delayed kinetics of expansion, as mice with conditional deletion of AMPKα1 displayed a lower percentage of OVA-specific T cells over the course of infection (Figure 7C). Re-stimulation of splenocytes from day 7 infected mice in vitro revealed a reduction in the number of IFN-γ$^+$CD8$^+$ (Figures 7D-E) and IFN-γ$^+$CD4$^+$ (Figure S7C) T cells in KO-T mice. At 3 dpi, bacterial load was elevated in the liver of infected KO-T mice compared to control animals and a similar trend was also observed in the spleens of infected mice (Figure S7D), suggesting reduced pathogen clearance in KO-T mice. No difference in the percentage of splenic CD8$^+$CD44^{hi}CD62L^{lo} (activated or Tem) cells was observed between genotypes, although there was a slight increase in the number of CD8$^+$CD44^{hi}CD62L^{hi} (Tcm) cells in the spleens of some KO-T mice (Figure S7E). CD44 expression on OVA-specific CD8$^+$ T cells (K^b/SIINFEKL) was similar between genotypes (Figure S7F), while CD8$^+$K^b/SIINFEKL T cells from KO-T mice displayed lower KLRG1

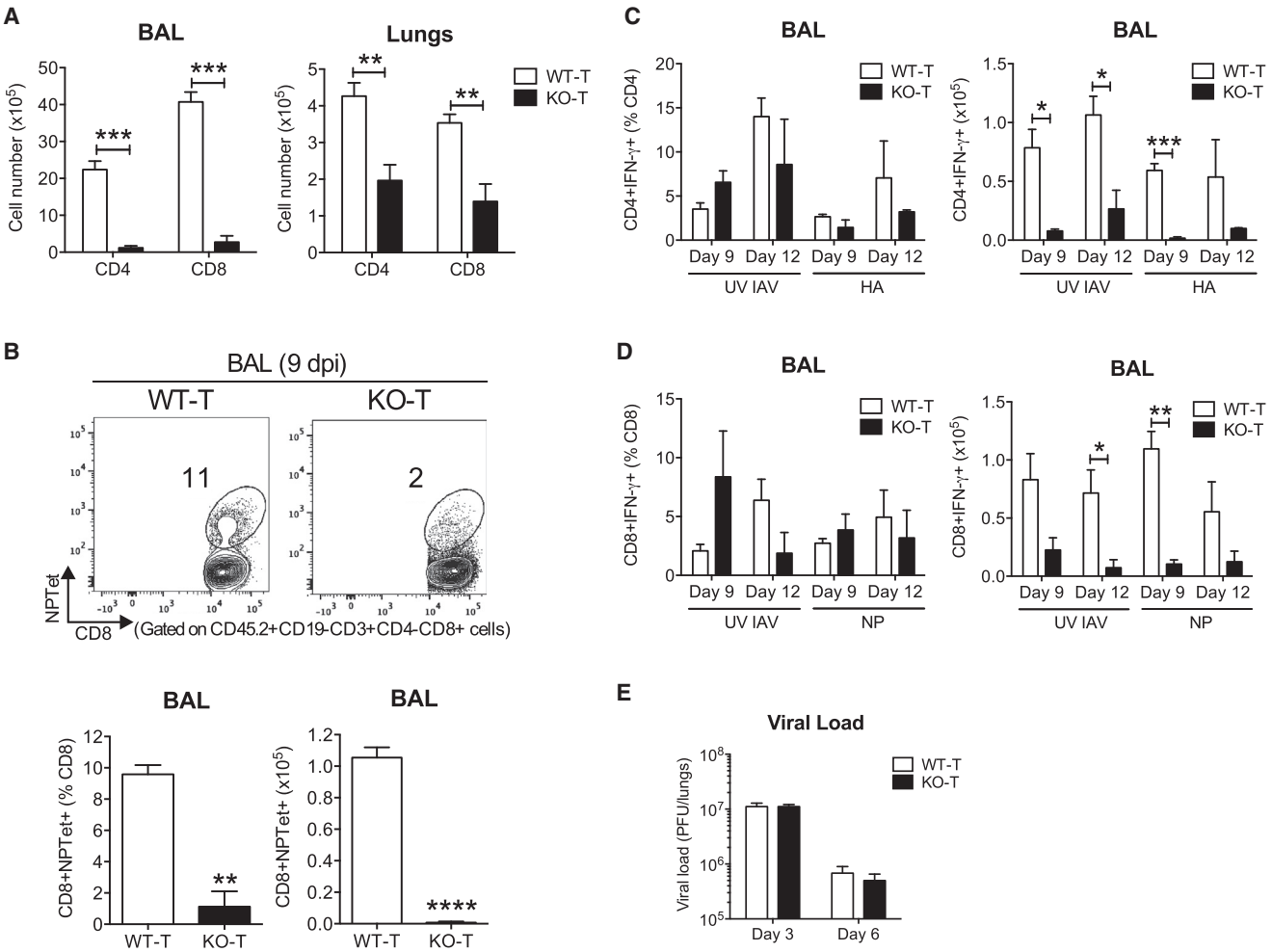

Figure 6. AMPKα1 Is Required for Primary T Cell Responses to Pulmonary Influenza A Viral Infection

(A) Total number of $CD4^+$ and $CD8^+$ T cells ($CD45.2^+CD19^-CD3^+$) in the BAL (left) and lungs (right) of control (WT-T) and T cell AMPKα1-deficient (KO-T) mice 9 days post infection (dpi).

(B) Flow cytometry analysis of IAV H-$2D^b$-NP^+CD8^+ T cells in the BAL of WT-T and KO-T mice at 9 dpi. Numbers indicate the percentage of $CD8^+$ T cells stained with NP-loaded H-$2D^b$ tetramer (NPTet). The frequency and total number of IAV H-$2D^b$-NP^+CD8^+ T cells in the BAL of WT-T and KO-T mice at day 9 post-infection are indicated.

(C and D) The frequency (left panel) and total number (right panel) of Ag-specific IFN-γ^+ $CD4^+$ (C) and $CD8^+$ (D) T cells from the BAL of infected WT-T and KO-T mice at 9 and 12 dpi was determined by ICS following 10 hr stimulation with UV-inactivated IAV (1 MOI), 5 μg/ml IAV $HA_{110–120}$ or IAV $NP_{366–374}$ peptides.

(E) Viral load in the lungs of infected WT-T and KO-T mice 3 and 6 dpi. All data are expressed as the mean ± SEM for 4–5 mice/group. *$p < 0.05$; **$p < 0.01$; ***$p < 0.001$; ****$p < 0.0001$.

expression (Figure S7G), suggesting a reduced number of short-lived effector cells (SLECs) in these animals.

To examine the importance of AMPKα1 on the survival of activated T cells in vivo, we adoptively transferred equal numbers of in vitro activated $CD8^+$OT-I^+ T cells isolated from either WT-T or KO-T ($Ly5.2^+$) mice into recipient congenic hosts ($Ly5.1^+$) that had been infected with wild-type *Lm* to generate an inflammatory, but antigen-irrelevant environment. The number of KO-T OT-$I^+Ly5.2^+$ donor cells recovered from the spleens of recipient mice was lower than that of AMPKα1-expressing control cells (Figure 7F), indicating reduced survival of AMPKα1-deficient $CD8^+$ T cells in inflammatory environments in vivo.

Finally, we assessed whether the genetic ablation of Raptor, a scaffolding protein for mTORC1 (Laplante and Sabatini, 2009), in T cells would rescue the defect in primary responses by AMPKα1-deficient T cells in vivo. Deletion of Raptor failed to reverse the phenotype of AMPKα1-deficient T cells, as mice harboring T cell specific deletion of both AMPKα1 and Raptor (DKO-T) failed to generate OVA-specific (Figures S7H and S7I) or IFN-γ-producing (Figure S7J) $CD8^+$ T cells after infection with *rLmOVA*.

AMPKα1-Deficient Teff Cells Display Reduced Metabolic Activity In Vivo

To examine whether the reduced ability of AMPKα1-deficient T cells to adapt to metabolic perturbations in vitro was linked to impaired generation of Teff cells in vivo we examined the metabolic profile of Teff cells from KO-T animals following

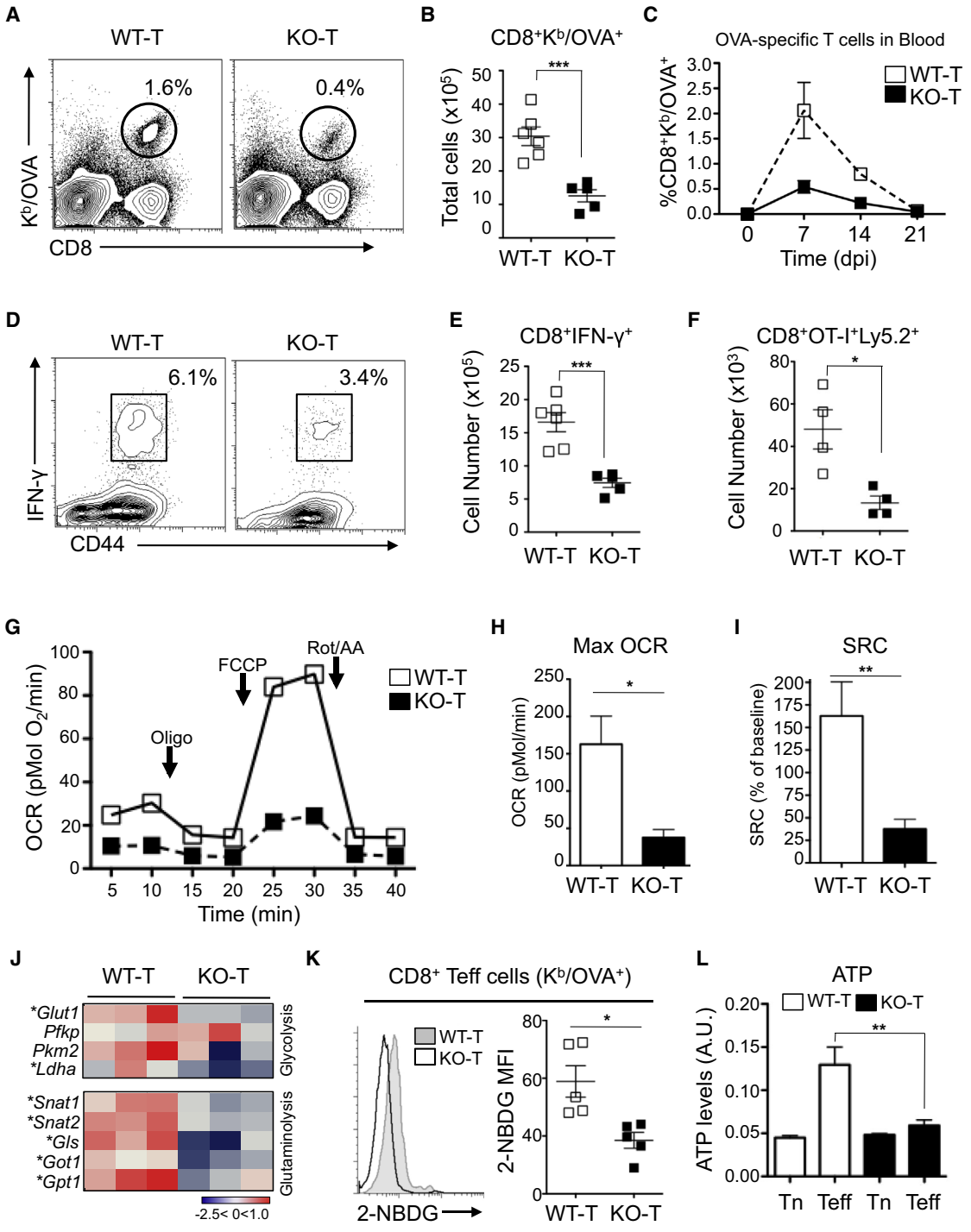

Figure 7. AMPKα1 Is Required for Primary T Cell Responses to *L. monocytogenes*

(A and B) Control (WT-T) and T cell AMPKα1-deficient (KO-T) mice were infected with *rLmOVA*, and splenocytes analyzed for antigen-specific responses 7 dpi. The percentage (A) and total number (B) of OVA-Tetramer (K^b/OVA)-positive $CD8^+$ T cells in spleens of infected mice at 7 dpi are indicated (WT-T, n = 6; KO-T, n = 5).

(C) The percentage of $CD8^+K^b/OVA^+$ T cells in peripheral blood was measured over time following infection of WT-T and KO-T mice with *rLmOVA*.

(D and E) Splenocytes from *rLmOVA*-infected mice were stimulated with OVA peptide 7 dpi, and IFN-γ production by $CD8^+$ T cells assessed by ICS. (D) CD44 versus IFN-γ staining for $CD8^+$ T cells. (E) Total numbers of $CD8^+$IFN-γ^+ T cells.

(F) WT-T and KO-T OT-I T cells ($Ly5.2^+$) were activated in vitro for 3 days, followed by adoptive transfer (6×10^6 cells/mouse) into $Ly5.1^+$ congenic hosts infected with wild-type *Lm* three days prior. Recovery of surviving $CD8^+$OT-$I^+Ly5.2^+$ T cells in the spleens of recipient mice 3 days post transfer are shown.

(legend continued on next page)

pathogenic challenge. WT-T and KO-T mice were infected with *rLmOVA* (as in Figure S7A), and activated CD8$^+$ Teff cells (CD44^{hi}CD62L^{lo}) were isolated 7 dpi and subjected to bioenergetic profiling ex vivo (Figures 7G–7I). CD8$^+$ Teff cells isolated from *LmOVA*-infected KO-T mice displayed reduced basal mitochondrial OCR relative to control T cells (Figure 7G). Moreover, the maximal mitochondrial oxidative capacity (Figure 7H) and SRC (Figure 7I) of AMPKα1-deficient *Lm*-specific CD8$^+$ Teff cells were reduced relative to control Teff cells.

To assess the impact of AMPKα1 on T cell metabolic reprogramming in vivo, we examined metabolic gene expression in Teff cells isolated from *rLmOVA*-infected mice. Teff cells from KO-T mice displayed reduced expression of glucose (*Glut1, Ldha*) and glutamine (*Snat1, Snat2, Gls, Got1, Gpt1*) metabolism genes (Figure 7J). We next measured glucose uptake by Teff cells in vivo using the fluorescent glucose analog 2-NBDG (O'Sullivan et al., 2014). While larger than conventional glucose due to its fluorescent tag, 2-NBDG is actively transported into cells similar to D-glucose and can be used to image glucose uptake in live cells (O'Neil et al., 2005). WT-T and KO-T mice were infected with *rLmOVA*, injected with 2-NBDG 7 dpi and 2-NBDG uptake by CD8$^+$K^b/ SIINFEKL$^+$ T cells in vivo was assessed by flow cytometry. 2-NBDG uptake by antigen-specific CD8$^+$ T cells from KO-T mice was ~30% lower relative to WT-T cells (Figure 7K). Finally, we measured ATP concentrations in CD8$^+$ T cells sorted from *rLmOVA*-infected mice (7 dpi). No difference in ATP concentrations was observed for naive T cells (CD44^{lo}CD62L^{hi}) of each genotype (Figure 7L). However, ATP concentrations were higher in Teff cells (CD44^{hi}CD62L^{lo}) from WT-T mice, while ATP concentrations in KO-T CD8$^+$ Teff cells were similar to naive T cells (Figure 7L). Together, these data indicate that AMPKα1 is required to maintain the metabolic homeostasis of Teff cells in vivo.

DISCUSSION

Much of our understanding of T cell metabolism is based on the metabolic programs engaged by Teff cells in vitro. Under these conditions, where nutrient availability is in excess relative to normal physiological concentrations, glycolytic metabolism (i.e., the Warburg effect) is a dominant metabolic program in Teff cells. However, our results indicated that Teff cells are capable of adapting their metabolism in response to reduced glucose availability, even in the presence of TCR-mediated metabolic reprogramming that favors glycolytic metabolism. We found that Teff cells actively engage glutamine-dependent OXPHOS to maintain ATP concentrations and cell viability under low glucose conditions. The energy sensor AMPK played a key role in this metabolic adaptation. AMPKα1-deficient T cells displayed reduced metabolic plasticity in response to glucose limitation in vitro, and reduced metabolic activity and lower ATP levels during pathogenic challenge in vivo. The reversible metabolic checkpoint induced in lymphocytes is reminiscent of AMPK function in tumor cells, where AMPK triggers a cell cycle checkpoint to maintain cell viability under poor nutrient conditions (Jones et al., 2005). We speculate that T cells display metabolic flexibility to help preserve cell viability and effector function in the face of varying environmental conditions.

Energetic homeostasis can be achieved by increasing ATP production or reducing energy expenditure. Our data suggested that Teff cells engage both strategies to adapt to glucose limitation. We found that T cells actively dampened energy-consuming processes including cell proliferation and cytokine production when nutrients were low. IFN-γ production was highly sensitive to glucose availability. Shifting Teff cells to physiological glucose concentrations (~5 mM) promoted a significant decrease in *Ifng* mRNA translation and overall IFN-γ production. AMPK acts as a key regulator of this process by suppressing cytokine mRNA translation under conditions of reduced glucose availability. Stimulation of AMPK activity by AICAR or phenformin actively suppressed IFN-γ production by Teff cells, while AMPKα1-deficient Teff cells appeared locked in a pro-growth state marked by increased IFN-γ production, even when metabolic conditions were unfavorable.

Conversely, we found that T cells actively engaged alternate pathways of ATP production to maintain T cell energetic homeostasis under conditions of metabolic stress. Glutamine-dependent OXPHOS was essential for maintaining T cell energetic homeostasis, as removal of glutamine promoted the rapid depletion of both TCA cycle intermediates and cellular ATP in Teff cells, even when glucose was readily available. These data argue against the Warburg effect as the main metabolic program for ATP production in activated T cells. Glucose starvation triggered an AMPKα1-dependent shift in Teff cell metabolic reprogramming by increasing the expression of genes involved in glutamine uptake and glutaminolysis (i.e., *Snat1, Snat2, Gls*). In addition, our SITA experiments indicate that T cells with low glycolytic flux can engage a novel metabolic shunt involving the conversion of glutamine to pyruvate. Engaging this metabolic shunt allows glucose-starved T cells to maintain a pool of pyruvate, derived from glutamine rather than glucose, which can be converted to acetyl-CoA and maintain TCA cycle homeostasis, similar to adaptive strategies used by glucose-starved tumor cells (Le et al., 2012; Yang et al., 2009). AMPK activity is required for these processes, as AMPKα1-deficient T cells are less able to engage glutamine oxidation to compensate for loss of glycolysis-derived ATP.

To date, the role of AMPK in T cell function has been controversial. T cells isolated from whole body AMPKα1-deficient

(G–I) Bioenergetic profile of *Lm*-specific Teff cells ex vivo. CD44^{hi}CD62L^{lo} CD8$^+$ T cells from WT-T (white) and KO-T (black) mice were sorted 7 dpi, and the (G) OCR profile following addition of mitochondrial inhibitors (oligomycin, FCCP, rotenone/antimycin A), (H) maximal mitochondrial OCR, and (I) SRC were determined by Seahorse analysis (n = 3 per genotype).

(J) Expression of glucose and glutamine metabolism genes by WT-T and KO-T CD8$^+$ Teff cells isolated from *rLmOVA*-infected mice 7 dpi. Data are expressed as the log2 fold change relative to naive control (CD44^{low}CD62L^{hi}) CD8$^+$ T cells isolated from *rLmOVA*-infected mice (n = 3 per genotype).

(K) In vivo 2-NBDG uptake by CD8$^+$K^b/OVA$^+$ cell from WT-T and KO-T mice 7 dpi. Left panel, representative histogram of 2-NBDG fluorescence for CD8$^+$K^b/OVA$^+$ T cells. Right panel, quantification of 2-NBDG MFI for T cells isolated from individual mice (n = 5 per genotype).

(L) ATP content of CD8$^+$ naive (Tn) and Teff cells isolated from *rLmOVA*-infected WT-T and KO-T mice 7 dpi. *$p < 0.05$; **$p < 0.01$; ***$p < 0.001$.

mice display normal responses to mitogenic stimulation in vitro (MacIver et al., 2011; Mayer et al., 2008), while impaired central memory T cell (Tcm) generation has been reported using an independent T cell-specific AMPKα1-deleted mouse strain (Rolf et al., 2013). These data are in sharp contrast with the murine model of whole-body AMPKα1 deletion, which leads to the accumulation of activated $CD8^+$ T cells (MacIver et al., 2011) and exacerbated T cell-mediated pathology in an in vivo model of autoimmunity (Nath et al., 2009). Using three distinct in vivo model systems, we provide evidence that AMPKα1 is required for primary T cell responses in vivo. Loss of AMPKα1 did not affect the differentiation of naive $CD4^+$ T cells into Th1 or Th17 cells in immunodeficient mice; rather, the total number of inflammatory *Prkaa1*$^{-/-}$ $CD4^+$ Teff cells that developed in recipient mice was dramatically reduced, leading to reduced development of T cell-mediated colitis. Similarly, the expansion of antigen-specific $CD8^+$ T cells in response to viral (IAV) or bacterial (*rLmOVA*) infection was reduced in animals lacking AMPKα1 expression in T cells, despite the fact that AMPKα1-deficient T cells displayed normal TCR-stimulated proliferation in vitro and homeostatic proliferation in vivo. The reduced number of AMPKα1-deficient Teff cells observed in all three model systems may reflect a failure of Teff cells to persist or survive in inflammatory microenvironments. In support of this, AMPKα1-deficient Teff cells displayed increased sensitivity to apoptosis when faced with nutrient limitation in vitro or inflammatory environments in vivo.

Our data point to AMPK-dependent control of T cell metabolism as a key determinant of T cell effector responses. While AMPKα1-deficient T cells displayed a lower ATP:AMP ratio relative to control T cells, AMPKα1 was not required for TCR-mediated proliferation or metabolic programming when glucose was in excess. Rather, AMPK was required to modulate T cell metabolism and effector function when glucose was scarce. Under low glucose conditions, *Prkaa1*$^{-/-}$ T cells displayed reduced levels of glutamine-dependent OXPHOS and were unable to maintain cellular ATP levels, leading to increased bioenergetic deficit and cell death. Similarly, AMPKα1-deficient Teff cells displayed reduced metabolic gene expression, lower glucose uptake, and reduced OXPHOS and mitochondrial SRC in response to pathogenic challenge in vivo. SRC represents increased mitochondrial electrochemical potential, which can be used to generate ATP, and is a key index of T cell metabolic fitness (Pearce and Pearce, 2013; van der Windt et al., 2012). Impaired nutrient utilization and reduced SRC may explain the failure of AMPKα1-deficient Teff cells to maintain cellular ATP concentrations, survive metabolic challenges in vitro, and mount robust effector responses in vivo.

Overall, our study provides evidence that T cells have evolved a rapid nutrient-sensing system that influences the metabolic fitness of responding Teff cells in vivo. This metabolic checkpoint—regulated by the energy sensor AMPK—ultimately influences the size (cell number) and strength (cytokine production) of the T cell response. We hypothesize that this intrinsic system evolved to maintain mitochondrial function and cellular energy levels in T cells to support the viability and phenotypic stability of Teff cells in microenvironments where O_2 and nutrients might be limiting. This raises the possibility that other metabolic sensors, such as HIF-1α (Wang and Green, 2012a) or mTOR (Powell and Delgoffe, 2010; Zeng and Chi, 2013), might regulate T cell effector function through similar effects on T cell bioenergetics. In this regard, AMPK agonists, such as metformin or A-769662 (Vincent et al., 2014), might provide new ways to shape T cell-mediated immune responses by altering T cell metabolism and mitochondrial function.

EXPERIMENTAL PROCEDURES

Mice

AMPKα1-deficient (*Prkaa1*$^{-/-}$), T cell AMPKα1-deficient (*Prkaa1*$^{fl/fl}$) and Raptor-deficient (*Rptr*$^{fl/fl}$), *Tcrb*$^{-/-}$, *Rag2*$^{-/-}$, OT-I, and C57BL/6-Ly5.1 mice were bred and maintained under specific pathogen-free conditions at McGill University under approved protocols.

T Cell Purification and Culture

$CD4^+$ and $CD8^+$ T cells were purified from spleen and peripheral lymph nodes by negative selection and cultured in T cell medium (TCM) containing IMDM supplemented with 10% FBS, L-glutamine, penicillin-streptomycin, and 2-ME as previously described (Jones et al., 2007; MacIver et al., 2011). For nutrient limitation conditions and SITA experiments, cells were cultured in TCM containing 10% dialyzed FBS.

Flow Cytometry

Single-cell suspensions were stained with fluorescently conjugated Abs as previously described (Jones et al., 2007; MacIver et al., 2011). Antigen-specific $CD8^+$ T cells were quantified using H2-K^bOVA$_{257–264}$ (K^b/OVA) or H-$2D^b$-NP tetramers. Cell viability was assessed using the Fixable Viability Dye eFluor® 780 (eBioscience). ICS was performed using specific fluorochrome-labeled mAbs (eBioscience) and flow cytometry as previously described (MacIver et al., 2011). For 2-NBDG uptake in vivo, mice were injected intravenously (i.v.) with 100 μg 2-NBDG/mouse 15 min prior to analysis (O'Sullivan et al., 2014). Flow cytometry was performed on a Gallios or LSR II flow cytometer and analyzed with FlowJo software.

Metabolic Assays

OCR, ECAR, and SRC were determined using a Seahorse XF96 Extracellular Flux Analyzer following established protocols (Chang et al., 2013). ATP levels were determined using CellTiter-Glo® Luminescent Cell Viability reagent (Promega). GC-MS- and LC-MS-based metabolomics studies were performed using previously described methods (Dupuy et al., 2013; Faubert et al., 2013). For SITA experiments, T cells were cultured with [U-^{13}C]-glucose or [U-^{13}C]-glutamine (Cambridge Isotope Laboratories) for 0.5–6 hr. Mass isotopomer distribution was determined using a custom algorithm developed at McGill University (McGuirk et al., 2013).

Immunoblotting and Quantitative Real-Time PCR

Immunoblotting and qPCR were conducted as previously described (MacIver et al., 2011). Protein lysates were generated using AMPK Lysis Buffer supplemented with protease and phosphatase inhibitors (Faubert et al., 2013). Primary and secondary Abs and qPCR primer sets are listed in Supplemental Experimental Procedures.

Adoptive Transfers and Infection Models

For development of T cell-mediated colitis, $CD4^+CD25^-$ T cells were transferred into *Tcrb*$^{-/-}$ or *Rag2*$^{-/-}$ recipient mice, and inflammatory infiltration into the cLP assessed 21 days later by flow cytometry and histological examination of H&E stained colon sections. Cytokine production in the mLN and cLP was determined by ICS. Histopathological scoring is described in Supplemental Experimental Procedures. Influenza A virus (IAV) infections were performed with mouse-adapted IAV H1N1 strain A/Puerto Rico/8/34 (PR8) as previously described (Coulombe et al., 2014). Mice were injected intravenously with a sublethal dose of *rLmOVA* (5×10^4 cfu/ml) as described (Jones et al., 2007). Mice were sacrificed 7 dpi, and splenocytes analyzed for the presence of OVA-specific $CD8^+$ T cells, cytokine production by $CD4^+$ and $CD8^+$ T cells by ICS, or $CD8^+CD44^{hi}CD62L^{lo}$ cells sorted for metabolic assays.

Statistical Analysis

Data are presented as mean ± SD for technical replicates, or mean ± SEM for biological replicates. Statistical significance is indicated in all figures by the following annotations: *p < 0.05; **p < 0.01; ***p < 0.001; ****p < 0.0001.

SUPPLEMENTAL INFORMATION

Supplemental Information includes seven figures and Supplemental Experimental Procedures and can be found with this article online at http://dx.doi.org/10.1016/j.immuni.2014.12.030.

ACKNOWLEDGMENTS

We thank Maya Poffenberger, Orval Mamer, and Eric Ma for review of the manuscript; Bozena Samborska, Rosalie Michaud, and Breanna Flynn for animal husbandry; and Daina Avizonis, Gaelle Bridon, and Luc Choiniere of the GCRC Metabolic Core Facility for technical support. Salary support from the Canadian Institutes of Health Research (CIHR, to R.G.J.), the Fonds de Recherche du Québec-Santé (FRQS, to J.B.), and the McGill Integrated Cancer Research Training Program (MICRTP, to J.B.) is acknowledged. Grant support was provided by the NIAID (5R01AI091965, to E.L.P.), the Arthritis Society (RG-11-017, to R.G.J.), and the CIHR (MOP-93799, to R.G.J.). This work is dedicated to the memory of Rosalind Goodman.

Received: January 15, 2014
Accepted: December 3, 2014
Published: January 2, 2015

REFERENCES

Ardawi, M.S., and Newsholme, E.A. (1983). Glutamine metabolism in lymphocytes of the rat. Biochem. J. *212*, 835–842.

Bensinger, S.J., Bradley, M.N., Joseph, S.B., Zelcer, N., Janssen, E.M., Hausner, M.A., Shih, R., Parks, J.S., Edwards, P.A., Jamieson, B.D., and Tontonoz, P. (2008). LXR signaling couples sterol metabolism to proliferation in the acquired immune response. Cell *134*, 97–111.

Brand, K. (1985). Glutamine and glucose metabolism during thymocyte proliferation. Pathways of glutamine and glutamate metabolism. Biochem. J. *228*, 353–361.

Carr, E.L., Kelman, A., Wu, G.S., Gopaul, R., Senkevitch, E., Aghvanyan, A., Turay, A.M., and Frauwirth, K.A. (2010). Glutamine uptake and metabolism are coordinately regulated by ERK/MAPK during T lymphocyte activation. J. Immunol. *185*, 1037–1044.

Cham, C.M., and Gajewski, T.F. (2005). Glucose availability regulates IFN-gamma production and p70S6 kinase activation in CD8+ effector T cells. J. Immunol. *174*, 4670–4677.

Cham, C.M., Driessens, G., O'Keefe, J.P., and Gajewski, T.F. (2008). Glucose deprivation inhibits multiple key gene expression events and effector functions in CD8+ T cells. Eur. J. Immunol. *38*, 2438–2450.

Chang, C.H., Curtis, J.D., Maggi, L.B., Jr., Faubert, B., Villarino, A.V., O'Sullivan, D., Huang, S.C., van der Windt, G.J., Blagih, J., Qiu, J., et al. (2013). Posttranscriptional control of T cell effector function by aerobic glycolysis. Cell *153*, 1239–1251.

Coulombe, F., Jaworska, J., Verway, M., Tzelepis, F., Massoud, A., Gillard, J., Wong, G., Kobinger, G., Xing, Z., Couture, C., et al. (2014). Targeted prostaglandin E2 inhibition enhances antiviral immunity through induction of type I interferon and apoptosis in macrophages. Immunity *40*, 554–568.

Dupuy, F., Griss, T., Blagih, J., Bridon, G., Avizonis, D., Ling, C., Dong, Z., Siwak, D.R., Annis, M.G., Mills, G.B., et al. (2013). LKB1 is a central regulator of tumor initiation and pro-growth metabolism in ErbB2-mediated breast cancer. Cancer & metabolism *1*, 18.

Faubert, B., Boily, G., Izreig, S., Griss, T., Samborska, B., Dong, Z., Dupuy, F., Chambers, C., Fuerth, B.J., Viollet, B., et al. (2013). AMPK is a negative regulator of the Warburg effect and suppresses tumor growth in vivo. Cell Metab. *17*, 113–124.

Frauwirth, K.A., Riley, J.L., Harris, M.H., Parry, R.V., Rathmell, J.C., Plas, D.R., Elstrom, R.L., June, C.H., and Thompson, C.B. (2002). The CD28 signaling pathway regulates glucose metabolism. Immunity *16*, 769–777.

Hardie, D.G., Ross, F.A., and Hawley, S.A. (2012). AMPK: a nutrient and energy sensor that maintains energy homeostasis. Nat. Rev. Mol. Cell Biol. *13*, 251–262.

Jacobs, S.R., Herman, C.E., Maciver, N.J., Wofford, J.A., Wieman, H.L., Hammen, J.J., and Rathmell, J.C. (2008). Glucose uptake is limiting in T cell activation and requires CD28-mediated Akt-dependent and independent pathways. J. Immunol. *180*, 4476–4486.

Jaramillo, M., Gomez, M.A., Larsson, O., Shio, M.T., Topisirovic, I., Contreras, I., Luxenburg, R., Rosenfeld, A., Colina, R., McMaster, R.W., et al. (2011). Leishmania repression of host translation through mTOR cleavage is required for parasite survival and infection. Cell Host Microbe *9*, 331–341.

Jaworska, J., Coulombe, F., Downey, J., Tzelepis, F., Shalaby, K., Tattoli, I., Berube, J., Rousseau, S., Martin, J.G., Girardin, S.E., et al. (2014). NLRX1 prevents mitochondrial induced apoptosis and enhances macrophage antiviral immunity by interacting with influenza virus PB1-F2 protein. Proc. Natl. Acad. Sci. USA *111*, E2110–E2119.

Jones, R.G., Plas, D.R., Kubek, S., Buzzai, M., Mu, J., Xu, Y., Birnbaum, M.J., and Thompson, C.B. (2005). AMP-activated protein kinase induces a p53-dependent metabolic checkpoint. Mol. Cell *18*, 283–293.

Jones, R.G., Bui, T., White, C., Madesh, M., Krawczyk, C.M., Lindsten, T., Hawkins, B.J., Kubek, S., Frauwirth, K.A., Wang, Y.L., et al. (2007). The proapoptotic factors Bax and Bak regulate T Cell proliferation through control of endoplasmic reticulum Ca(2+) homeostasis. Immunity *27*, 268–280.

Krawczyk, C.M., Shen, H., and Pearce, E.J. (2007). Functional plasticity in memory T helper cell responses. J. Immunol. *178*, 4080–4088.

Laplante, M., and Sabatini, D.M. (2009). mTOR signaling at a glance. J. Cell Sci. *122*, 3589–3594.

Le, A., Lane, A.N., Hamaker, M., Bose, S., Gouw, A., Barbi, J., Tsukamoto, T., Rojas, C.J., Slusher, B.S., Zhang, H., et al. (2012). Glucose-independent glutamine metabolism via TCA cycling for proliferation and survival in B cells. Cell Metab. *15*, 110–121.

Macintyre, A.N., Gerriets, V.A., Nichols, A.G., Michalek, R.D., Rudolph, M.C., Deoliveira, D., Anderson, S.M., Abel, E.D., Chen, B.J., Hale, L.P., and Rathmell, J.C. (2014). The glucose transporter Glut1 is selectively essential for CD4 T cell activation and effector function. Cell Metab. *20*, 61–72.

MacIver, N.J., Blagih, J., Saucillo, D.C., Tonelli, L., Griss, T., Rathmell, J.C., and Jones, R.G. (2011). The liver kinase B1 is a central regulator of T cell development, activation, and metabolism. J. Immunol. *187*, 4187–4198.

MacIver, N.J., Michalek, R.D., and Rathmell, J.C. (2013). Metabolic regulation of T lymphocytes. Annu. Rev. Immunol. *31*, 259–283.

Mayer, A., Denanglaire, S., Viollet, B., Leo, O., and Andris, F. (2008). AMP-activated protein kinase regulates lymphocyte responses to metabolic stress but is largely dispensable for immune cell development and function. Eur. J. Immunol. *38*, 948–956.

McGuirk, S., Gravel, S.P., Deblois, G., Papadopoli, D.J., Faubert, B., Wegner, A., Hiller, K., Avizonis, D., Akavia, U.D., Jones, R.G., et al. (2013). PGC-1alpha supports glutamine metabolism in breast cancer. Cancer & metabolism *1*, 22.

McNamee, E.N., Korns Johnson, D., Homann, D., and Clambey, E.T. (2013). Hypoxia and hypoxia-inducible factors as regulators of T cell development, differentiation, and function. Immunol. Res. *55*, 58–70.

Michalek, R.D., Gerriets, V.A., Jacobs, S.R., Macintyre, A.N., MacIver, N.J., Mason, E.F., Sullivan, S.A., Nichols, A.G., and Rathmell, J.C. (2011a). Cutting edge: distinct glycolytic and lipid oxidative metabolic programs are essential for effector and regulatory CD4+ T cell subsets. J. Immunol. *186*, 3299–3303.

Michalek, R.D., Gerriets, V.A., Nichols, A.G., Inoue, M., Kazmin, D., Chang, C.Y., Dwyer, M.A., Nelson, E.R., Pollizzi, K.N., Ilkayeva, O., et al. (2011b). Estrogen-related receptor-α is a metabolic regulator of effector T-cell activation and differentiation. Proc. Natl. Acad. Sci. USA *108*, 18348–18353.

Nakaya, M., Xiao, Y., Zhou, X., Chang, J.H., Chang, M., Cheng, X., Blonska, M., Lin, X., and Sun, S.C. (2014). Inflammatory T Cell Responses Rely on

Amino Acid Transporter ASCT2 Facilitation of Glutamine Uptake and mTORC1 Kinase Activation. Immunity *40*, 692–705.

Nath, N., Khan, M., Rattan, R., Mangalam, A., Makkar, R.S., de Meester, C., Bertrand, L., Singh, I., Chen, Y., Viollet, B., and Giri, S. (2009). Loss of AMPK exacerbates experimental autoimmune encephalomyelitis disease severity. Biochem. Biophys. Res. Commun. *386*, 16–20.

O'Neil, R.G., Wu, L., and Mullani, N. (2005). Uptake of a fluorescent deoxyglucose analog (2-NBDG) in tumor cells. Molecular imaging and biology: MIB: the official publication of the Academy of Molecular Imaging *7*, 388–392.

O'Sullivan, D., van der Windt, G.J., Huang, S.C., Curtis, J.D., Chang, C.H., Buck, M.D., Qiu, J., Smith, A.M., Lam, W.Y., DiPlato, L.M., et al. (2014). Memory CD8(+) T cells use cell-intrinsic lipolysis to support the metabolic programming necessary for development. Immunity *41*, 75–88.

Owen, O.E., Kalhan, S.C., and Hanson, R.W. (2002). The key role of anaplerosis and cataplerosis for citric acid cycle function. J. Biol. Chem. *277*, 30409–30412.

Pearce, E.L., and Pearce, E.J. (2013). Metabolic pathways in immune cell activation and quiescence. Immunity *38*, 633–643.

Pearce, E.L., Walsh, M.C., Cejas, P.J., Harms, G.M., Shen, H., Wang, L.S., Jones, R.G., and Choi, Y. (2009). Enhancing CD8 T-cell memory by modulating fatty acid metabolism. Nature *460*, 103–107.

Powell, J.D., and Delgoffe, G.M. (2010). The mammalian target of rapamycin: linking T cell differentiation, function, and metabolism. Immunity *33*, 301–311.

Rolf, J., Zarrouk, M., Finlay, D.K., Foretz, M., Viollet, B., and Cantrell, D.A. (2013). AMPKα1: a glucose sensor that controls CD8 T-cell memory. Eur. J. Immunol. *43*, 889–896.

Sinclair, L.V., Rolf, J., Emslie, E., Shi, Y.B., Taylor, P.M., and Cantrell, D.A. (2013). Control of amino-acid transport by antigen receptors coordinates the metabolic reprogramming essential for T cell differentiation. Nat. Immunol. *14*, 500–508.

Sitkovsky, M., and Lukashev, D. (2005). Regulation of immune cells by local-tissue oxygen tension: HIF1 alpha and adenosine receptors. Nat. Rev. Immunol. *5*, 712–721.

Sukumar, M., Liu, J., Ji, Y., Subramanian, M., Crompton, J.G., Yu, Z., Roychoudhuri, R., Palmer, D.C., Muranski, P., Karoly, E.D., et al. (2013). Inhibiting glycolytic metabolism enhances CD8+ T cell memory and antitumor function. J. Clin. Invest. *123*, 4479–4488.

van der Windt, G.J., Everts, B., Chang, C.H., Curtis, J.D., Freitas, T.C., Amiel, E., Pearce, E.J., and Pearce, E.L. (2012). Mitochondrial respiratory capacity is a critical regulator of CD8+ T cell memory development. Immunity *36*, 68–78.

van der Windt, G.J., O'Sullivan, D., Everts, B., Huang, S.C., Buck, M.D., Curtis, J.D., Chang, C.H., Smith, A.M., Ai, T., Faubert, B., et al. (2013). CD8 memory T cells have a bioenergetic advantage that underlies their rapid recall ability. Proc. Natl. Acad. Sci. USA *110*, 14336–14341.

Vincent, E.E., Coelho, P.P., Blagih, J., Griss, T., Viollet, B., and Jones, R.G. (2014). Differential effects of AMPK agonists on cell growth and metabolism. Oncogene. Published online September 22, 2014. http://dx.doi.org/10.1038/onc.2014.301.

Wang, R., and Green, D.R. (2012a). Metabolic checkpoints in activated T cells. Nat. Immunol. *13*, 907–915.

Wang, R., and Green, D.R. (2012b). Metabolic reprogramming and metabolic dependency in T cells. Immunol. Rev. *249*, 14–26.

Wang, R., Dillon, C.P., Shi, L.Z., Milasta, S., Carter, R., Finkelstein, D., McCormick, L.L., Fitzgerald, P., Chi, H., Munger, J., and Green, D.R. (2011). The transcription factor Myc controls metabolic reprogramming upon T lymphocyte activation. Immunity *35*, 871–882.

Wu, M., Neilson, A., Swift, A.L., Moran, R., Tamagnine, J., Parslow, D., Armistead, S., Lemire, K., Orrell, J., Teich, J., et al. (2007). Multiparameter metabolic analysis reveals a close link between attenuated mitochondrial bioenergetic function and enhanced glycolysis dependency in human tumor cells. Am. J. Physiol. Cell Physiol. *292*, C125–C136.

Yang, C., Sudderth, J., Dang, T., Bachoo, R.M., McDonald, J.G., and DeBerardinis, R.J. (2009). Glioblastoma cells require glutamate dehydrogenase to survive impairments of glucose metabolism or Akt signaling. Cancer Res. *69*, 7986–7993.

Zeng, H., and Chi, H. (2013). mTOR and lymphocyte metabolism. Curr. Opin. Immunol. *25*, 347–355.